CrossMark

Ejection of small droplet from microplate using focused ultrasound

Hiroki Tanaka*, Yosuke Mizuno, and Kentaro Nakamura

Laboratory for Future Interdisciplinary Research of Science and Technology, Tokyo Institute of Technology, Yokohama 226-8503, Japan

*E-mail: htanaka@sonic.pi.titech.ac.jp

We discussed an ultrasonic system for single-droplet ejection from a microplate, which is one of the basic and important procedures in the noncontact handling of droplets in air. In this system, a 1.5 MHz concave transducer located below the microplate is used for chasing the liquid surface through a pulse echo method, and also for the ejection of a 1 μL single droplet by the burst of focused ultrasound. We investigated the relationship between the droplet ejection characteristics, the distance from the transducer to the surface of liquid, the material property, and the excitation condition of the focused ultrasonic transducer. It was verified that the optimal position of the transducer was off the focal point of sound pressure by ±1 mm, because the sound intensity had to be controlled to eject a single droplet. Subsequently, we confirmed experimentally that the ejected droplet volume linearly depended on the surface tension of the liquid, and that the droplet volume and ejection velocity were determined by the Webber number, Reynolds number, and Ohnesolge number. In addition, by optimizing the duration of the burst ultrasound, the droplet volume and ejection velocity were controlled. © 2017 The Japan Society of Applied Physics

1. Introduction

The noncontact handling of small components, powders, and droplets is thought as a key technology in future pharmacy industry as well as in novel material science and engineering. Several trials for the noncontact manipulation of object have been reported to be based on air pressure[1] and magnetic/electric fields considering various applications.[2,3] Compared with these methods, ultrasonic levitation, which is based on the phenomenon that objects smaller than the wavelength are trapped at the sound pressure nodal points of the standing wave field, has advantages in tranquility, cost efficiency, and applicability to nonelectric/magnetic objects, and has attracted considerable attention.[4–11] In the meantime, the ultrasonic manipulation of small particles or cells in liquid has been extensively studied by many research groups.[12–14]

The authors have set a research goal to implement all the procedures of noncontact transport of objects, especially droplets, in air based on ultrasonic radiation force, namely, injection, linear transport, direction switching, mixing, ejection, analysis, and dispensing. We can utilize the kinetic effect of ultrasonic waves in handling small objects in air.[15–24] Although the linear transport,[25–27] direction switching,[28] mixing,[29] ejection from the trapped state,[30] and dispensing[31,32] have already been demonstrated to some extent, the ejection of a droplet from a well must be studied to accomplish the goal.

The ejection of a droplet has been researched since 1970s as "drop-on-demand" or "acoustic drop ejection technology (ADE)", which was performed by irradiating focused ultrasound to a free liquid surface.[33] This technology has been developed also for nozzleless inkjet printing[34–37] and liquid handling in life science.[38–42] In these previous research studies, the number and volume of droplets were controlled by adjusting the tone burst of focused ultrasound. The transfer of nanoliter droplets from one microplate to the other was also reported.

In this paper, we discuss a system for droplet ejection from one of the wells in a microplate. The scheme of transducer positioning based on liquid surface chasing by a pulse echo method is proposed. The droplet ejection characteristics of the system are evaluated as functions of the distance from the transducer to the surface of liquid, the material property, and the excitation condition of the focused ultrasonic transducer.
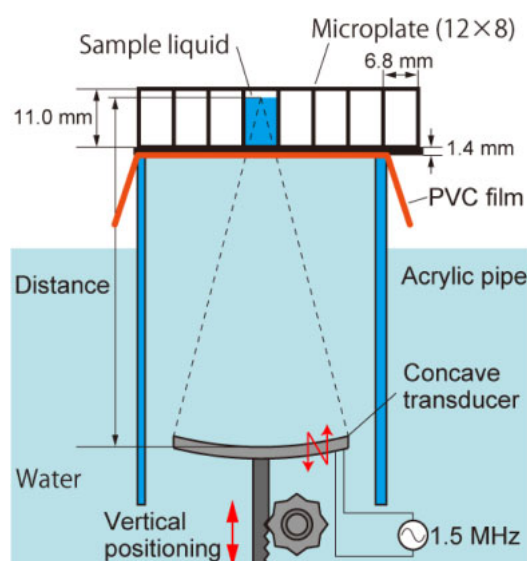

Fig. 1. (Color online) Ejection system for droplet from microplate.

2. Droplet ejection system

2.1 Configuration of ejection system

Figure 1 illustrates the ejection system to be discussed in this paper. A concave transducer with a radius of curvature of 60 mm and an aperture diameter of 30 mm is located below a microplate, and driven with 1.5 MHz tone-burst waves. The microplate has 96 wells. The diameter and depth of each well are 6.8 and 11.0 mm, respectively. The ultrasound waves are focused at the surface of liquid contained in the well across the bottom of the microplate. The thickness of the bottom is 1.4 mm. An acrylic pipe is used to support the microplate. A thin poly(vinyl chloride) (PVC) film is set at the top end of the pipe to confine water inside the pipe.

2.2 Ejection scheme procedure considered in this paper

The procedure of the droplet ejection system for the microplate consists of three steps as shown in Fig. 2. In the first step, the distance from the transducer to the surface of liquid is estimated by a pulse echo method at room temperature (20–25 °C). The concave transducer for the ejection is used also for pulse–echo measurement. In the second step,
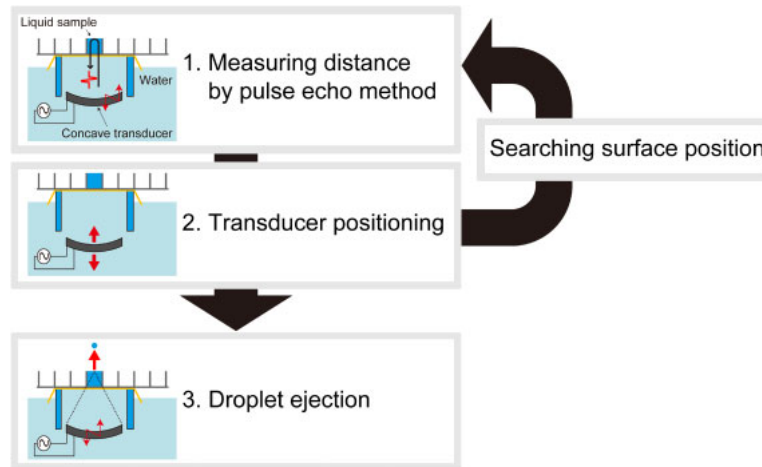
Fig. 2. (Color online) Schematic procedure of noncontact droplet ejection system.

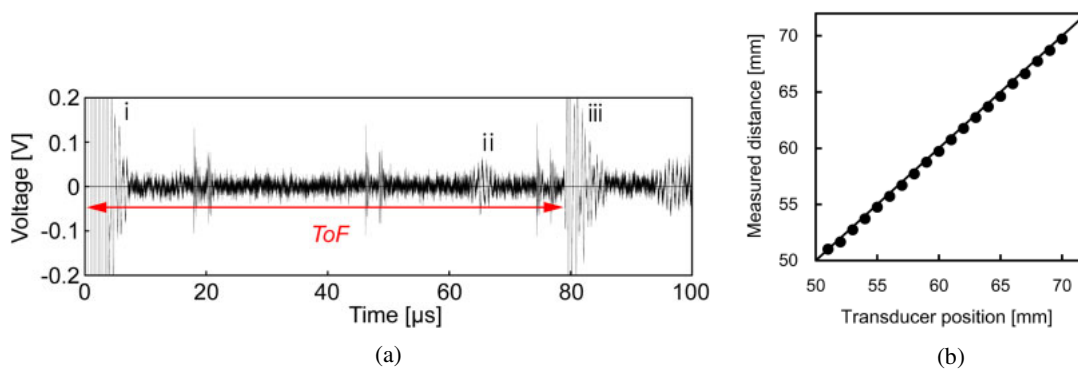(a)   (b)

Fig. 3. (Color online) (a) Echo signal received at the transducer positioned 63.5 mm relative to the liquid surface and (b) distance measured from the transducer to the liquid surface by pulse echo method.

the position of the transducer is adjusted according to the result of the pulse–echo measurement. In the third step, a droplet is ejected.

2.3 Distance measurement between liquid surface and transducer

The distance between the liquid surface and the transducer was measured by a pulse echo method from 51.0 to 70.0 mm in 1.0 mm steps. One of the wells of the microplate was filled with water. The transducer was driven by a single cycle of sinusoidal voltage of 60 V. Figure 3(a) shows the signal received by the same transducer when the distance from the transducer to the surface of liquid was set at 60 mm. The waves indicated with i, ii, and iii correspond to the driving signal, the reflected signals from the bottom of the well, and the surface of liquid, respectively. The durations of the waves were increased by the ringing of the transducer due to its resonance. The short spikes observed between these ultrasound signals are thought to be attributed to electrical reflections in the cable. The time between the driving signal and the reflected signal from the surface was measured as the time-of-flight (ToF) by zero-crossing detection. Using the ToF, the distance D (from the transducer to the surface of liquid) was calculated as

$$D = \frac{C_w \, \text{ToF}}{2} + \left(1 - \frac{C_w}{C_p}\right)d, \qquad (1)$$

considering the thickness of the microplate bottom, d. The microplate is made of polystyrene. Here, C_w and C_p are the

sound speeds in water and polystyrene, respectively. C_w, C_p, and d are 1500 m/s, 2340 m/s, and 1.45 mm, respectively. The distance measured by the pulse echo method is plotted as the actual distance as shown in Fig. 3(b). The distance from the transducer to the surface of liquid was successfully estimated over the whole range considered. The amplitude of the pulse reflected from the liquid surface was measured along the central axis of the transducer as shown in Fig. 4(a). The square of the envelope amplitude is plotted as the normalized sound intensity in the figure. The blue line indicates the normalized theoretical sound intensity calculated from the sound pressure $p(t, r)$ at the distance r on the transducer central axis:[43]

$$p(t,r)$$

$$= \begin{cases} \rho c \dfrac{R_0}{R_0 - r}\left[u\left(t - \dfrac{r}{C_w}\right) - u\left(t - \dfrac{R}{C_w}\right)\right] & (r < R_0) \\[3mm] \dfrac{\rho a^2}{2R_0}\alpha\left(t - \dfrac{R_0}{C_w}\right) & (r = R_0) \\[3mm] \rho c \dfrac{R_0}{R_0 - r}\left[u\left(t - \dfrac{R}{C_w}\right) - u\left(t - \dfrac{r}{C_w}\right)\right] & (r > R_0) \end{cases}.$$

$$(2)$$

Here, R_0 is the radius of curvature of the transducer, a is the transducer aperture radius, and $u(t)$ and $\alpha(t)$ represent the vibration velocity and acceleration of the transducer, respectively. Continuous sinusoidal waves are applied for $u(t)$ and $\alpha(t)$. Note that the focal point of sound intensity exists at the
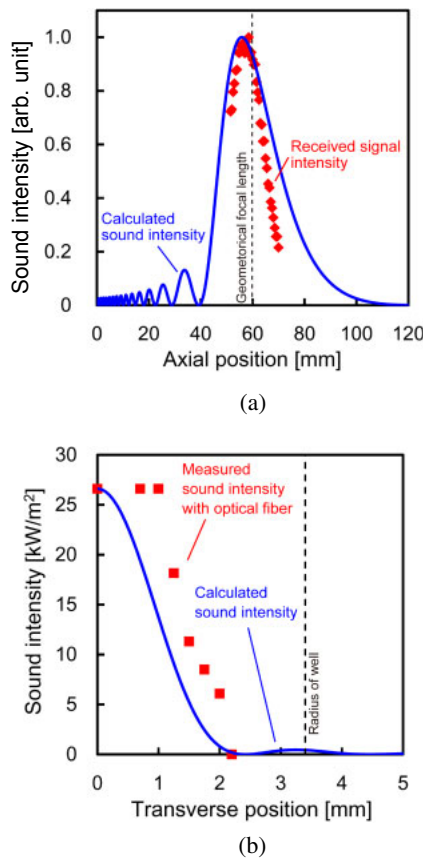
(a)

(b)

Fig. 4. (Color online) Sound intensity distribution along (a) the axis of the transducer and (b) transverse direction from the center across the focal position.

Fig. 5. (Color online) Experimental images of droplet ejection taken with shutter speed of $1/20{,}000$ s and frame rate of 2,000 fps.

distance of $r \sim 58$ mm, which is smaller than the geometrical focal length $R_0 = 60$ mm. The sound intensity of 50% of that at the focal point is reserved for ± 5 mm in front and at the back of the focus. Subsequently, we measured the transverse distribution of sound intensity in the focal area. A thin optical fiber needle hydrophone for detecting the reflectivity change at the fiber end according to the sound pressure[44–46] was used. The measured sound intensity is shown in red in Fig. 4(b), while the distribution given by the following approximate equation[47] is drawn using a blue line.

$$p(\theta) \propto \frac{J_1(ka\sin\theta)}{ka\sin\theta} \qquad (3)$$

Here, k is the wave number ($= 2\pi/\lambda$) and J_1 is the Bessel function of the first kind. Most of the acoustic power is confined in the area with a diameter of 3–4 mm, which is sufficiently smaller than the diameter of the well. The position drift of the fiber end due to the circulation of the water induced by acoustic streaming might cause measurement error.

3. Ejection of droplet

3.1 Trajectory of droplet

Figure 5 shows the images of the ejection of a water droplet taken using a high-speed camera with a frame rate of 2,000 fps (frames per second) and a shutter speed of $1/20{,}000$ s. The distance between the liquid surface and the transducer was set at 60 mm, and the duration of excitation was 5 ms. The time t was measured from the start of surface deformation. As observed in Fig. 5, the area corresponding to the
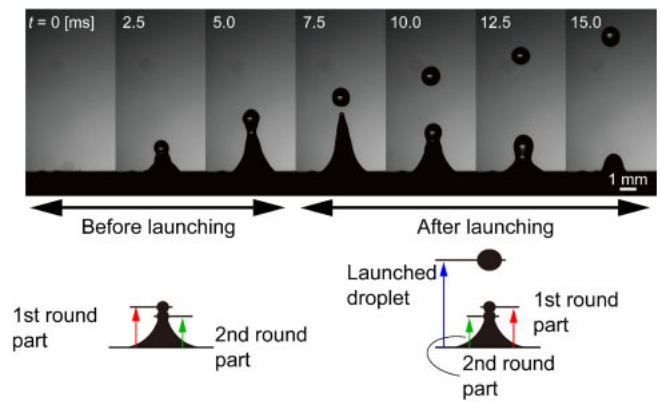
focused region was deformed, and the acoustic intensity in this area was estimated to be higher than $12 \, \text{kW/m}^2$ using the measured sound intensity. Thus, the acoustic power applied to the liquid surface was approximately 0.1 W by the contour integration of the acoustic intensity distribution.

At $t = 2.5$ ms, part of the liquid surface protrudes steeply and the protrusion is composed of two round parts. At $t = 7.5$ ms, the first part is pinched off and launched as a droplet. At $t = 10.0$ ms, the remaining liquid surface deforms into two round parts. Figure 6(a) shows the vertical positions of the centers of the round part and the launched droplet. Blue circles, red squares, and green triangles represent the centers of the launched droplet and the first and second round parts, respectively. The first round part departed at around $t = 7.5$ ms and continued to fly upward, and the trajectory is plotted in the figure. As the surface of the droplet was oscillating, we fitted the shape with an ellipse and recorded its center as the trace. Before the droplet separated, the wavelength of liquid surface deformation, which is the distance between two round parts, was 1 mm, and after the separation, the wavelength became 0.7–2.2 mm. The capillary length κ^{-1} is defined as the characteristic length scale for an interface subject to gravity and surface tension. The surface wave of fluid can be recognized as the capillary wave if the wavelength is larger than the capillary length ($\lambda \ll 2\pi\kappa^{-1}$), otherwise the gravity wave ($\lambda \gg 2\pi\kappa^{-1}$). The capillary length κ^{-1} is defined as

$$\kappa^{-1} = \sqrt{\frac{\sigma}{\rho g}}, \qquad (4)$$

where σ is the surface tension, ρ is the density, and g is the acceleration of gravity. The wavelengths observed are much smaller than $2\pi\kappa^{-1} = 17.1$ mm; thus, the wave of the liquid surface is considered as the capillary wave. Figure 6(b) shows the vertical velocities of the first (blue) and second centers after the droplet was pinched off (red). The maximal deformation velocity of the surface of liquid was 1.0 m/s, and the ejection velocity was 0.5 m/s. On average, the liquid surface deformed at the velocity of 0.68 m/s, and after the droplet ejection, 0.40 m/s. The phase velocity of the capillary wave, c, can be calculated as

$$c = \sqrt{\frac{g}{k} + \frac{\sigma k}{\rho}}, \qquad (5)$$
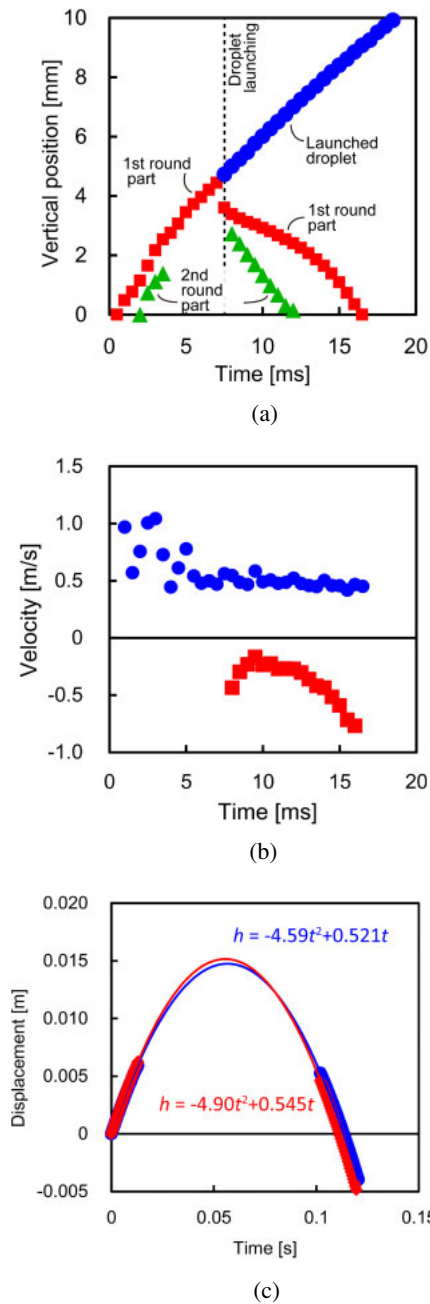
(a)

(b)

(c)

Fig. 6. (Color online) (a) Vertical positions of ejected droplets (blue) and heights of liquid surfaces of first (red) and second centers (green). (b) Velocities of first center (blue) and second center after droplet was pinched off (red). (c) Comparison of droplet trajectory measured after the pinching off (blue) and that calculated from the pinching off velocity (red).

where k $(= 2\pi/\lambda)$ is the wave number. The phase velocities calculated to be 0.65 and 0.45–0.84 m/s before and after the droplet separation, respectively, using Eq. (5) with the measured wavelength of the surface wave are in good agreement with the measured deformation velocities. Thus, the droplet pinching off is thought to be caused by, or at least, enhanced by the capillary wave.

Next, we observed the droplet trajectory after the pinching off and compared it with the theoretical vertical position $h(t)$:

$$h(t) = -\frac{1}{2}gt^2 + v_0 t, \qquad (6)$$
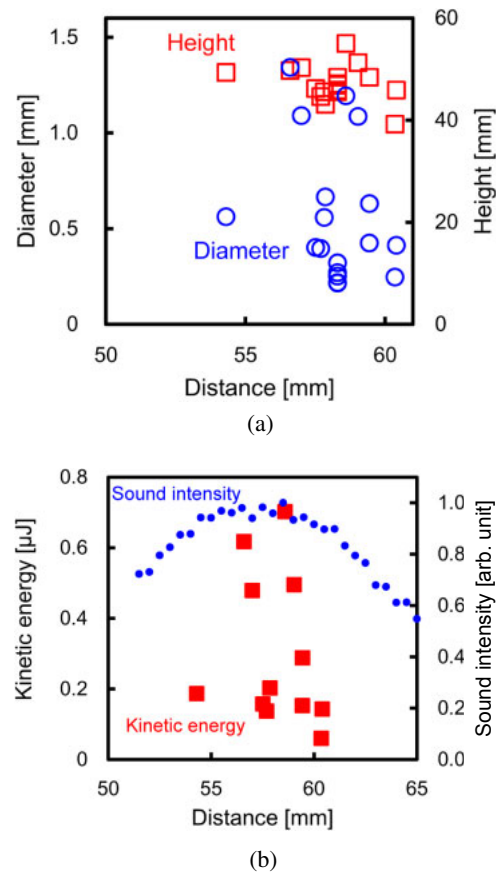

(a)

(b)

Fig. 7. (Color online) (a) Ejection height (red squares, right scale) and diameter (blue circles, left scale) of droplet, and (b) dependences of sound intensity (blue circles, right scale) and kinetic energy (red squares, left scale) of droplet on distance from transducer to liquid surface.

where v_0 is the pinching-off velocity of the droplet. Figure 6(c) shows the measured and calculated trajectories. The droplet position is estimated from the pinching-off velocity using Eq. (6).

3.2 Distance from transducer to liquid surface and ejection characteristics

We verified the relationship between the droplet volume, the ejection height, and the distance from the transducer to the surface of liquid. The driving voltage and current were set to 62 V and 6.5 A, respectively. The distance from the transducer to the surface of liquid was varied from 53.0 to 63.0 mm in 0.1 mm steps. The diameter and velocity of the ejected droplet were measured with a high-speed camera. The ejection height, which is the highest position reached, was calculated on the basis of the energy conservation law. The distance from the transducer to the surface of liquid was measured by the pulse echo method. Figure 7(a) shows the measured droplet diameter and ejection height. At the distance of 58 mm, which corresponds to the experimental focal length, the ejected droplet diameter and ejection height decreased. In contrast, at the distances of 57 and 59 mm, the droplet diameter and ejection height were maximum. This is because a very high sound power was irradiated and caused multiple droplet ejection or nebulizing. The kinetic energy of the droplet was calculated using the measured droplet diameter and ejection velocity as shown in Fig. 7(b). At the distances of 57 and 59 mm, the kinetic energy was also maximum.
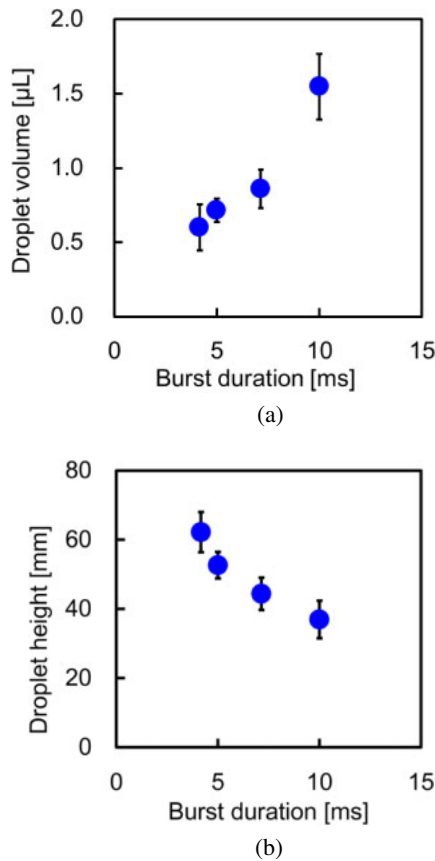
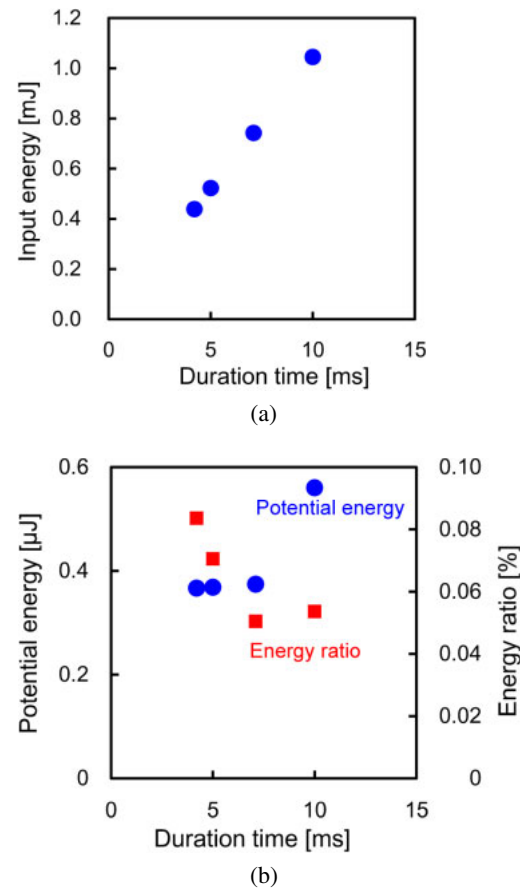Fig. 8. (Color online) Dependences of (a) ejected water droplet volume and (b) height on burst duration.

Fig. 9. (Color online) (a) Dependence of acoustic energy on burst duration and (b) potential energy of ejected droplet (blue circles, left scale) and energy ratio of potential energy to acoustic energy (red squares, right scale).

3.3 Burst duration and ejection characteristics

Here, we verified the relationship between the droplet volume, the ejection height, and the duration of the burst ultrasound. The droplet was ejected five times with different burst durations of 4.2, 5.0, 7.1, and 10.0 ms with the distance from the transducer to the surface of liquid of 60.0 mm. The driving voltages were 33.0, 29.6, 24.4, and 28.0 V, which were optimized for the durations of 4.2, 5.0, 7.1, and 10.0 ms, respectively, so that only a single droplet can be ejected. If the duration is increased by keeping the driving voltage constant, the satellite droplets tend to be easily ejected because of the increase in irradiated sound pressure. The droplet diameter and height were measured five times from the images taken with a digital video camera. The droplet volume was estimated using the measured diameter at the peak of its trajectory, assuming that the droplet is spherical at the peak. Figures 8(a) and 8(b) show the dependences of the droplet volume and height on the duration of the ultrasonic irradiation. When we changed the duration, 0.5–2.0 μL droplets were ejected. As the duration increased, the droplet volume also increased. At a duration longer than 10 ms, multiple droplets were likely generated. The ejection height decreased from 60 to 30 mm with increasing duration of the burst. When the ejection height was 50 mm, the ejection velocity was estimated to be around 1 m/s on the basis of the energy conservation law. Considering that the irradiated acoustic power to the liquid surface was 0.1 W, the acoustic energy was calculated as a function of the duration as shown in Fig. 9(a). The potential energy of the droplet was calculated as shown in Fig. 9(b) according to the ejected droplet volume and ejection

height. As the input acoustic energy increased, the potential energy of the ejected droplet also increased, in contrast to the energy ratio. Here, the energy ratio is defined as the ratio of the potential energy to the acoustic energy.

4. Material property and ejection characteristics

Next, we studied the dependence of the ejection characteristics on the liquid properties such as surface tension and viscosity. According to the previous research on the falling droplet from a syringe, the volume V_g is proportional to the surface tension σ as[48]

$$V_g = \frac{2\pi R_s}{\alpha_R g \rho} \sigma, \tag{7}$$

where R_s is the syringe radius and α_R is a function of the syringe and droplet radii. Thus, we expect that the ejected droplet volume will also linearly depend on the surface tension. On the other hand, inkjet characteristics can be evaluated with three dimensionless quantities: We, Weber number; Re, Reynolds number; Oh, Ohnesorge number;[49]

$$We = \frac{\rho v^2 L}{\sigma}, \tag{8}$$

$$Re = \frac{\rho v L}{\eta}, \tag{9}$$

$$Oh = \frac{\sqrt{We}}{Re} = \frac{\eta}{\sqrt{\rho \sigma L}}, \tag{10}$$
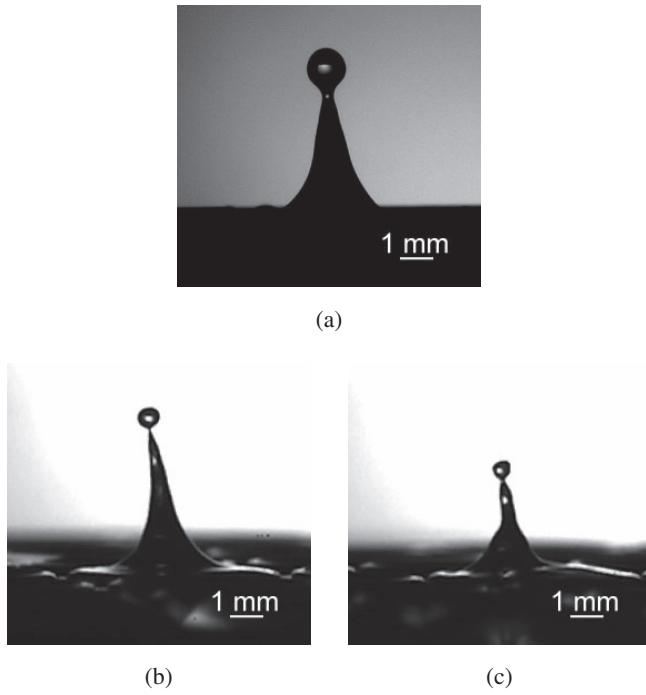
(a)

(b)　　　　　　　　　　　　(c)

Fig. 10. (a) Photos of ejected water, (b) ethanol, and (c) silicone oil droplets taken with shutter speed of $1/10,000$ s and frame rate of $1,000$ fps.

Table I. Physical properties at 25 °C and experimental results of droplet ejection.[51,52]

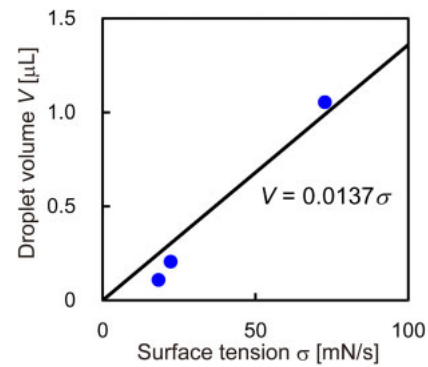|	Water	Ethanol	Silicone oil
Density ρ (kg/m^3)	997	789	873
Surface tension σ (mN/m)	72.0	22.0	18.3
Shear viscosity η (mPa s)	0.890	1.08	1.75
Ejection velocity v (m/s)	0.951	0.446	0.896
Droplet diameter d (mm)	1.263	0.733	0.592
Droplet volume V (μL)	1.054	0.206	0.109

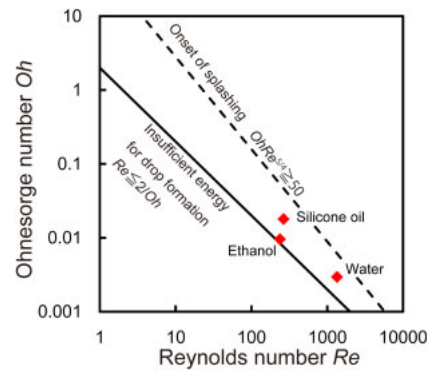**Fig. 11.** (Color online) Dependence of ejected droplet volume on surface tension.

Fig. 12. (Color online) Experimental results plotted in schematic diagram for drop-on-demand inkjet printing presented in Ref. 50.

where v is the velocity of the droplet jet, L is the droplet diameter, and η is the viscosity of the droplet. The Weber number (the ratio of the inertial force to the surface tension force) indicates the stability of the jetting droplet surface; the Reynolds number (the ratio of the inertial force to the viscous force) indicates the flow pattern of the liquid; the Ohnesorge number indicates the ratio of the viscous force to the square root of the product of the inertia and the surface tension force. The inkjet characteristics can be estimated by plotting the dependence of the Ohnesorge number on the Reynolds number in a log–log chart similar to that in Fig. 5 of Ref. 50. For example, in the area of $Re \leq 2/Oh$, the droplet has a sufficient kinetic energy for ejection. In the area of $Oh\,Re^{5/4} \geq 50$, the energy of the droplet is too large to eject a single droplet, thereby causing multiple droplet ejection or splashing.[50]

We measured the droplet ejection characteristics for the following three liquids: water, ethanol, and silicone oil. The viscosity of the silicone oil was 1.75 mPa·s (Shin-Etsu Silicone KF-96L-2cs). The driving current was set to 1.2 A, and the distance from the transducer to the surface of liquid was 60 mm. The ultrasound was irradiated for 5 ms. The ejected droplet diameter L, volume V, and velocity v were measured five times with a high-speed camera. Figures 10(a)–10(c) show the photos of the ejected water, ethanol, and silicone oil droplets, respectively. Table I shows the material properties of sample liquids and the measured L, V, and v averages. It is observed from the photos that the droplet volume and ejection height decreased as the surface tension of the liquid decreased. Figure 11 shows the dependence of the droplet volume on the surface tension. As expected from the previous research on the volume of the droplet falling from a syringe,[48] the volume of the ultrasonically ejected droplet also linearly depends on the surface tension.

To estimate the droplet ejection characteristics, the Ohnesorge and Reynolds numbers of water, ethanol, and silicone oil droplets are plotted in Fig. 5 of Ref. 50, as shown in Fig. 12. The area between the solid and dashed lines indicates the condition for the single droplet ejection according to the study on inkjet technology. The three results for the ultrasonic ejection in this study fell in this area. It can be concluded that the ejection characteristics are also estimated from these thresholds. If we know the surface tension and viscosity of the target liquid, the droplet volume can be controlled by changing the ejection velocity. In addition, these three results fall in the area of "satellite droplets",[50] and thus it is necessary to control the irradiation time and the amplitude of ultrasound to eject a single droplet.

5. Conclusions

We investigated the ultrasonic droplet ejection, which is one of the important procedures used in the noncontact ultrasonic manipulation of droplets. By irradiating a focused MHz ultrasound from a place below the bottom of the microplate,

a single droplet was successfully ejected from the liquid surface in the microplate. Ejection characteristics were discussed by changing the focusing position. Pulse echo measurement was introduced to detect the sample surface position. The relationship between the ejection characteristics and the liquid properties was investigated. We indicated that the droplet volume and ejection velocity can be controlled by optimizing the duration of burst ultrasound. We believe that these results provide some basic information necessary to design an ejection system for various sample liquids, and thus realize noncontact ultrasonic transport systems in the future.

Acknowledgements

1) S. Konishi, M. Harada, Y. Ogami, Y. Daiho, Y. Mita, and H. Fujita, ETFA 6th Int. Conf., 1997, p. 232.
2) S. Mukhopadhyay, J. Donaldson, G. Sengupta, S. Yamada, C. Chakraborty, and D. Kacprzak, IEEE Trans. Magn. **39**, 3220 (2003).
3) F. Hellman, E. M. Gyorgy, D. W. Johnson, H. M. O'Bryan, and R. C. Sherwood, J. Appl. Phys. **63**, 447 (1988).
4) R. R. Whymark, Ultrasonics **13**, 251 (1975).
5) E. G. Lierke, Acustica **82**, 220 (1996).
6) H. Hatano, Y. Kanai, Y. Ikegami, T. Fujii, and K. Sato, Nippon Onkyo Gakkaishi **47**, 40 (1991) [in Japanese].
7) E. Benes, M. Groschl, H. Nowotny, F. Trampler, T. Keijzer, H. Bohm, S. Radel, L. Gherardini, J. J. Hawkes, R. Konig, and Ch. Delouvroy, Proc. IEEE Ultrasonics Symp., 2001, p. 649.
8) Y. Hashimoto, Y. Koike, and S. Ueha, J. Acoust. Soc. Am. **103**, 3230 (1998).
9) Y. Hashimoto, Y. Koike, and S. Ueha, J. Acoust. Soc. Am. **100**, 2057 (1996).
10) R. Yano, M. Aoyagi, H. Tamura, and T. Takano, Jpn. J. Appl. Phys. **50**, 07HE29 (2011).
11) Y. Yamayoshi and S. Hirose, Jpn. J. Appl. Phys. **50**, 07HE28 (2011).
12) T. Kozuka, K. Yasui, S. Hatanaka, T. Tuziuti, K. Suzuki, and A. Towata, Jpn. J. Appl. Phys. **50**, 07HE27 (2011).
13) K. Masuda, R. Nakamoto, N. Watarai, R. Koda, Y. Taguchi, T. Kozuka, Y. Miyamoto, T. Kakimoto, S. Enosawa, and T. Chiba, Jpn. J. Appl. Phys. **50**, 07HF11 (2011).
14) M. Takeuchi and K. Yamanouchi, Jpn. J. Appl. Phys. **33**, 3045 (1994).
15) A. Haake and J. Dual, Ultrasonics **42**, 75 (2004).
16) T. Kozuka, K. Yasui, T. Tuziuti, A. Towada, and Y. Iida, Jpn. J. Appl. Phys. **46**, 4948 (2007).
17) T. Kozuka, K. Yasui, T. Tuziuti, A. Towada, and Y. Iida, Jpn. J. Appl. Phys. **47**, 4336 (2008).
18) J. Hawkes, J. Cefai, D. Barrow, W. Coakley, and L. Briarty, J. Phys. D **31**, 1673 (1998).
19) W. Coakley, J. Hawkes, M. Sobanski, C. Cousins, and J. Spengler, Ultrasonics **38**, 638 (2000).
20) A. Haake and J. Dual, J. Acoust. Soc. Am. **117**, 2752 (2005).
21) A. Osumi, K. Doi, and Y. Ito, Jpn. J. Appl. Phys. **50**, 07HE30 (2011).
22) K. Matsumoto and H. Miura, Jpn. J. Appl. Phys. **51**, 07GE05 (2012).
23) Y. Ochiai, T. Hoshi, and J. Rekimoto, PLOS ONE **9**, e97590 (2014).
24) M. A. B. Andrade, N. Pérez, and J. C. Adamowski, Appl. Phys. Lett. **106**, 014101 (2015).
25) D. Koyama and K. Nakamura, IEEE Trans. Ultrason. Ferroelectr. Freq. Control **57**, 1152 (2010).
26) Y. Ito, D. Koyama, and K. Nakamura, Acoust. Sci. Technol. **31**, 420 (2010).
27) M. Ding, D. Koyama, and K. Nakamura, Appl. Phys. Express **5**, 097301 (2012).
28) D. Koyama and K. Nakamura, IEEE Trans. Ultrason. Ferroelectr. Freq. Control **57**, 1434 (2010).
29) R. Nakamura, Y. Mizuno, and K. Nakamura, Jpn. J. Appl. Phys. **52**, 07HE02 (2013).
30) S. Murakami, D. Koyama, and K. Nakamura, AIP Conf. Proc. **1433**, 783 (2012).
31) H. Tanaka, Y. Wada, Y. Mizuno, and K. Nakamura, Jpn. J. Appl. Phys. **52**, 100201 (2013).
32) H. Tanaka, Y. Wada, Y. Mizuno, and K. Nakamura, Jpn. J. Appl. Phys. **55**, 067302 (2016).
33) K. A. Krause, IBM Tech. Disclosure Bull. **16**, 1168 (1973).
34) K. T. Lovelady and L. F. Toye, U.S. Patent 4,308,547 (1989).
35) S. A. Elrod, B. Hadimioglu, B. T. Khuri-Yakub, E. G. Rawson, E. Richley, C. F. Quate, N. N. Mansour, and T. S. Lundgren, J. Appl. Phys. **65**, 3441 (1989).
36) B. Hadimioglu, S. A. Elrod, M. Lim, D. L. Steinmetz, J. C. Zesch, B. T. Khuri-Yakub, E. G. Rawson, and C. F. Quate, IS&T's 8th Int. Congr. Advances in Non-Impact Printing Technologies, 1992, p. 411.
37) T. Hamazaki and N. Morita, J. Fluid Sci. Technol. **4**, 25 (2009).
38) E. Litborn, M. Stjernstrom, and J. Roeraade, Anal. Chem. **70**, 4847 (1998).
39) S. Hislip, G. P. Thomas, B. M. Manning, R. O'Kennedy, S. Edwards, and D. Diamond, Proc. SPIE **3857**, 174 (1999).
40) R. N. Ellson, Drug Discovery Today **7**, S32 (2002).
41) R. N. Ellson, presented at Nanotech and Biotech Convergence Conf., 2003.
42) R. N. Ellson, M. Mutz, B. Browning, L. Lee, Jr., M. F. Miller, and R. Papen, J. Lab. Autom. **8**, 29 (2003).
43) *Choonpa Binran* (Ultrasonics Handbook), ed. Choonpa Binran Henshu Iinkai (Maruzen, Tokyo, 1999) p. 38 [in Japanese].
44) J. Staudenraus and W. Eisenmenger, Ultrasonics **31**, 267 (1993).
45) J. F. Eykman, Recl. Trav. Chim. Pays-Bas **14**, 185 (1895).
46) H. Takei, T. Hasegawa, K. Nakamura, and S. Ueha, Jpn. J. Appl. Phys. **46**, 4555 (2007).
47) J. Saneyoshi, Y. Kikuchi, and O. Nomoto, *Choonpa Gijutsu Binran* (Handbook of Ultrasonic Techniques) (Nikkan-Kogyo, Tokyo, 1978) p. 167 [in Japanese].
48) X. D. Shi, M. P. Brenner, and S. R. Nagel, Science **265**, 219 (1994).
49) S. Schiaffino and A. A. Sonin, Phys. Fluids **9**, 3172 (1997).
50) G. H. McKinley and M. Renardy, Phys. Fluids **23**, 127101 (2011).
51) National Astronomical Observatory of Japan, *Rika Nenpyo* (Chronological Science Tables) (Maruzen, Tokyo, 1993) [in Japanese].
52) *Kagaku Binran* (Chemical Handbook, Basic Edition), ed. Chemical Society of Japan (Maruzen, Tokyo, 2004) 5th ed., Chap. II-94 [in Japanese].